SPECIAL TOPIC — Phononics and phonon engineering

First principles calculations on the thermoelectric properties of bulk Au_2S with ultra-low lattice thermal conductivity*

Y Y Wu(伍义远)[1,2,3,†], X L Zhu(朱雪良)[2,3,†], H Y Yang(杨恒玉)[4], Z G Wang(王志光)[5], Y H Li(李玉红)[1,‡], and B T Wang(王保田)[2,3,6,§]

[1] School of Nuclear Science and Technology, Lanzhou University, Lanzhou 730000, China
[2] Institute of High Energy Physics, Chinese Academy of Sciences, Beijing 100049, China
[3] Spallation Neutron Source Science Center, Dongguan 523808, China
[4] School of Materials Science and Engineering, Hunan University of Science and Technology, Xiangtan 411201, China
[5] Institute of Modern Physics, Chinese Academy of Sciences, Lanzhou 730000, China
[6] Collaborative Innovation Center of Extreme Optics, Shanxi University, Taiyuan 030006, China

(Received 30 March 2020; revised manuscript received 26 May 2020; accepted manuscript online 28 May 2020)

Sulfide nanocrystals and their composites have shown great potential in the thermoelectric (TE) field due to their extremely low thermal conductivity. Recently a solid and hollow metastable Au_2S nanocrystalline has been successfully synthesized. Herein, we study the TE properties of this bulk Au_2S by first-principles calculations and semiclassical Boltzmann transport theory, which provides the basis for its further experimental studies. Our results indicate that the highly twofold degeneracy of the bands appears at the Γ point in the Brillouin zone, resulting in a high Seebeck coefficient. Besides, Au_2S exhibits an ultra-low lattice thermal conductivity (~ 0.88 W·m^{-1}·K^{-1} at 700 K). At 700 K, the thermoelectric figure of merit of the optimal p-type doping is close to 1.76, which is higher than 0.8 of ZrSb at 700 K and 1.4 of PtTe at 750 K. Our work clearly demonstrates the advantages of Au_2S as a TE material and would greatly inspire further experimental studies and verifications.

Keywords: first principles calculation, thermodynamic transport properties

PACS: 72.15.Jf, 84.60.Rb **DOI:** 10.1088/1674-1056/ab973c

1. Introduction

In order to realize human's requirements for the sustainable development of future energy, we need to develop new and environmentally friendly renewable energy conversion technologies. Among them, temperature difference power generation is an effective energy technology. It uses the Seebeck effect of thermoelectric (TE) materials to directly convert waste heat into electrical energy without the need for mechanical moving parts and chemical reactions.[1,2] Due to its small size, lightweight, long service life, easy control, and pollution-free, TE materials have become one of the hotspots in international materials research.[3–5]

The efficiency of a TE material is mainly determined by the value $ZT = S^2\sigma T/(\kappa_e + \kappa_l)$, where S, T, σ, κ_e, and κ_l are the Seebeck coefficient, absolute temperature, electrical conductivity, electron thermal conductivity, and lattice thermal conductivity, respectively.[6–8] Since strong connections are universal among these transport coefficients, it is difficult to optimize all the transport coefficients at the same time to obtain a designed ZT value. Currently used strategies to improve ZT include increasing the power factor ($S^2\sigma$) or reducing the thermal conductivity. For example, band structure engineering has been used to improve $S^2\sigma$,[9,10] and nanostructure engineering (nanostructuring, modulation doping, etc.) has been proven to effectively reduce the thermal conductivity.[11–16] Among them, nanostructuring is considered to be a promising method and can be realized by the following three ways: (i) reducing the grain size to nanoscale;[12,17–19] (ii) introducing nanocrystals into nanomaterial hosts;[20,21] (iii) introducing nanoparticles into bulk hosts.[22,23] These approaches effectively help people to ease the complex competitive relationships among those transport parameters.

Metallic sulfide nanomaterials have been widely studied in recent years as a new class of TE materials due to their advantages in modification of nanostructuring. For example, bismuth sulfide (Bi_2S_3),[24] copper rich sulfides (Cu_2S, $Cu_{1.98}S$, $Cu_{1.97}S$),[25–28] silver sulfide (Ag_2S),[29,30] and SnS[31] have been experimentally synthesized and proved to exhibit good

*Project supported by the National Natural Science Foundation of China (Grant Nos. 11504312, 11775102, and 11805088), the National Basic Research Program of China (Grant No. 2015CB921103), China Postdoctoral Science Foundation (Grant No. 2018M641477), Guangdong Provincial Department of Science and Technology, China (Grant No. 2018A0303100013), and the Fundamental Research Funds for the Central Universities, China (Lanzhou University, Grant No. lzujbky-2018-19).

†These authors contributed equally to this work.
‡Corresponding author. E-mail: liyuhong@lzu.edu.cn
§Corresponding author. E-mail: wangbt@ihep.ac.cn

TE responses. In addition, a lot of works (such as doping or synthesizing nanocomposites) have been done to improve their TE conversion efficiency. Tarachand *et al.*[29] investigated the effect of silver nano-inclusions on TE properties of Ag_2S semiconducting nanostructures, and observed a significantly improved TE power factor for Ag_2S. Furthermore, they proved that the introduction of 10 vol% of Ag_2S metal nanoparticles in metallic CuS results in an increase of ZT by $\sim 37\%$.[20] Zheng *et al.*[30] prepared a series of p-type Ag-doped PbS compounds using vacuum melting combined with subsequent spark plasma sintering process, and found that the ZT value was doubled compared to that of the original PbS. All these studies show that metal sulfide nanomaterials have great potential as the ideal next-generation TE energy conversion materials.

Bulk Au_2S is a cuprite type compound similar to α-Ag_2S that has been experimentally synthesized.[32–34] Recently, Dalmases *et al.*[35] prepared solid and hollow metastable Au_2S nanocrystal by sequential cation exchange reactions. Such solid and hollow Au_2S nanocrystal may be applied to nanostructure engineering to obtain some nanocomposites with good TE properties. Furthermore, Au_2S may have the same low intrinsic thermal conductivity as Ag_2S due to their similar crystal structure and the large mass of the Au atom. Combining all these characteristics, we consider that Au_2S may have a good prospect in TE applications. The TE properties of Au_2S have not been reported experimentally and theoretically. In this paper, we use first-principles calculations and semiclassical Boltzmann transport theory to study the TE properties of bulk Au_2S. Our results may provide forceful theoretical basis for experiments in the future and could help to encourage further experiments in TE and related fields.

2. Computational methods

The electronic properties of bulk Au_2S are calculated based on density functional theory (DFT), which is implemented in the VASP.[36] Scalar relativistic projector augmented wave (PAW) pseudopotentials[37] and generalized gradient approximation of Perdew–Burke–Ernzerhof (PBE)[38] to the exchange–correlation functional are used. The s^1d^{10} and s^2p^4 atomic orbitals are treated as the valence states for the Au and S atoms, respectively. The cutoff energy is set as 550 eV. $7\times7\times7$ Monkhorst–Pack k-mesh is employed in the Brillouin-zone. The convergence criterion for electronic self-consistency is set to 10^{-5} eV. The forces on the atoms are smaller than 0.01 eV·Å^{-1}.

The electronic transport properties are obtained by the semiclassical Boltzmann transport theory and the rigid band approach, implemented in the BoltzTraP code.[39] The constant scattering time approximation is used to calculate the constant relaxation time. This is valid if the scattering time does not vary strongly with the energy on a scale of k_BT.[40] In order to obtain accurate Fourier interpolation of the Kohn–Sham eigenvalues, the k-mesh of $25\times25\times25$ is employed in the Brillouin region. The Boltzmann transport equation as implemented in ShengBTE code[41] is used to evaluate the phonon transport properties. The VASP and Phonopy packages[42] are used to obtained Harmonic phonons. The $2\times2\times2$ supercell and $5\times5\times5$ k-mesh are used for calculation. The third-order force constants (3rd IFCs) are calculated using the same supercells by a finite displacement approach. The 3rd IFCs consider the interaction including the sixth nearest neighbor atoms. Here, the convergence of κ_l is carefully tested with respect to the k-grids. This system uses a $11\times11\times11$ k-grid with good convergence.

3. Results and discussion

3.1. Crystal and band structure of bulk Au_2S

Bulk Au_2S belongs to the cubic crystal system, space group Pn-3m (No. 224), and its unit cell contains two formula units [4 Au and 2 S, as shown in Fig. 1(a)]. Four Au atoms are bonded around the central S atoms. The S–Au–S and Au–S–Au bond angles are 180.0° and 109.645°, respectively. Our optimized lattice parameters are $a=b=c=5.33$ Å, which are similar to Suárez's[43] calculation results ($a=b=c=5.34$ Å) and slight larger than Ishikawa's[34] experimental values ($a=b=c=5.02$ Å). To our knowledge, the electronic band of bulk Au_2S has not been reported in experiments. The optical band gap of colloidal Au_2S nanoparticles was experimentally measured to be 1.8 ± 0.2 eV,[33] which falls within the theoretically proposed range of 1.3–2.6 eV.[44] Suárez *et al.*[43] reported that the PBE functional is well adapted to describe the Au_2S system. Because the band gap computed at the HSE06 level is 3.0 eV, clearly overestimating the gap, we only use the PBE function to calculate the band of Au_2S. As seen in Fig. 1(b), bulk Au_2S is a semiconductor with a direct band gap of 1.95 eV, which is similar to Suárez's[43] calculation (1.94 eV). Both the valence band maximum (VBM) and the conduction band minimum (CBM) are located at the Γ point. A twofold degeneracy of the valence band (VB) primarily originates from the d-orbital of Au. Such kind of degeneracy is the key for achieving high ZT,[45] and indicates excellent p-type thermoelectric performance.[46] In addition, the relatively flat degenerate state at the edge of the valence band is beneficial to obtain higher Seebeck coefficients.[47] When the sizes of the materials are reduced to the nanoscale, the quantum constraint effect will have an effect on ZT. Generally, the sharp peaks in the density of electronic states (DOS) often result in a high $S^2\sigma$.[48–50] From the DOS of Au_2S in Fig. 1(b), several sharp peaks are observed at the VB, which are beneficial to its electronic transport properties.

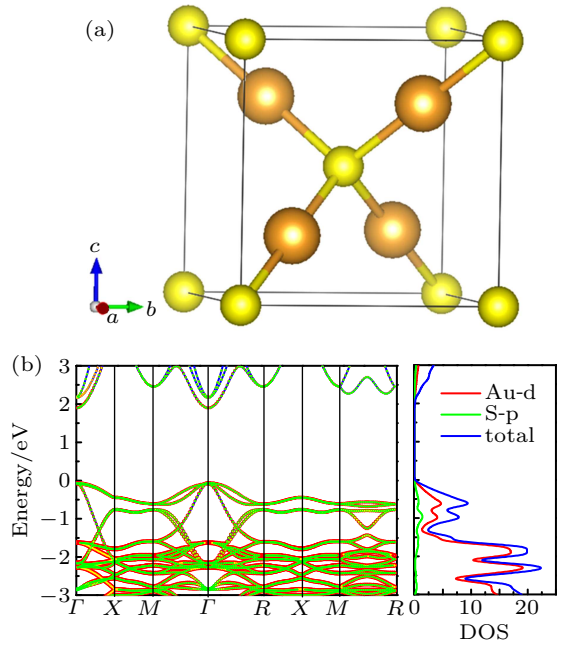

Fig. 1. (a) Crystal structure of bulk Au_2S (Au: orange; S: yellow). (b) Total and partial densities of states and band structure of Au_2S calculated with PBE. The Fermi level is set at zero.

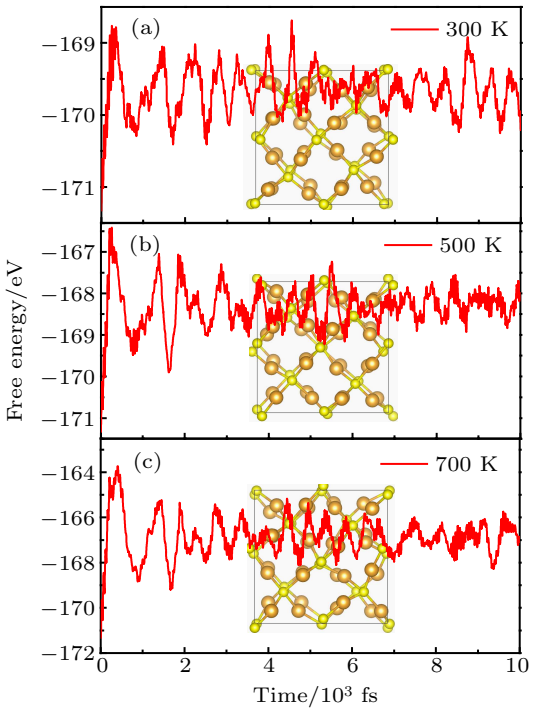

Fig. 2. Free energy fluctuation and the final structure of Au_2S in AIMD simulations at 300 K, 500 K, and 700 K.

To examine the stability of bulk Au_2S at high temperature, we perform the *ab initio* molecular dynamics (AIMD) simulation at 300 K, 500 K, and 700 K with a time step of 1 fs. As shown in Fig. 2, the free energy of the system fluctuates slightly in a range of stable values during the simulation process at 300 K, 500 K, and 700 K. Besides, the illustrations show that the crystal structure of Au_2S is well kept after heated for 10000 fs. As seen in Fig. 3, with the increase of temperature, the radius distribution function (RDF) of S–S, Au–Au, and Au–Au between 1–10 Å maintains a certain peak value, indicating that Au_2S maintains a long-term sequence at 300–700 K. Each of these peaks has a broadening due to the strong vibrations of the particles near the lattice point at evaluated temperatures. These results clearly prove that Au_2S can maintain structural stability even up to 700 K.

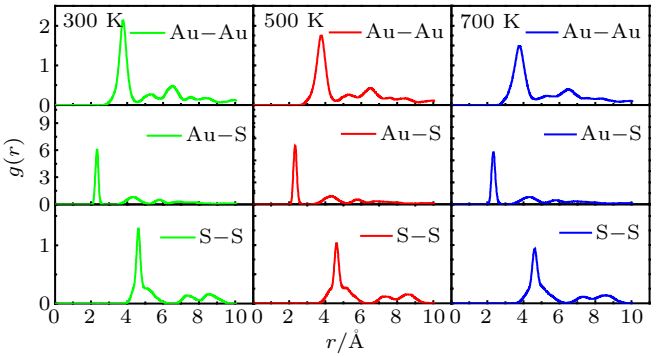

Fig. 3. The RDF of Au_2S at 300 K, 500 K, and 700 K.

3.2. Electrical transport properties

To evaluate the TE performance of bulk Au_2S, we systematically study the electronic transport coefficients (S, σ, and κ_e) using the Boltzmann transport theory. The electrical transport coefficients as functions of the chemical potential (μ) and temperature (T) are given by[39]

$$S_{\alpha\beta}(T,\mu) = \frac{1}{eTV\sigma_{\alpha\beta}(T,\mu)}\int \Sigma_{\alpha\beta}(\varepsilon)(\varepsilon-\mu) \times\left[-\frac{\partial f_\mu(T,\varepsilon)}{\partial\varepsilon}\right]\mathrm{d}\varepsilon, \quad (1)$$

$$\sigma_{\alpha\beta}(T,\mu) = \frac{1}{V}\int \Sigma_{\alpha\beta}(\varepsilon)\left[-\frac{\partial f_\mu(T,\varepsilon)}{\partial\varepsilon}\right]\mathrm{d}\varepsilon, \quad (2)$$

where α, β, ε, and V are the Cartesian indices, energy, and the volume of the unit cell, respectively. $\Sigma_{\alpha\beta}(\varepsilon)$ is the transport distribution function and can be defined as

$$\Sigma_{\alpha\beta}(\varepsilon) = \frac{e^2}{N_0}\sum_{i,q}\tau_e \upsilon_\alpha(i,q)\,\upsilon_\beta(i,q)\,\frac{\delta(\varepsilon-\varepsilon_{i,q})}{d\varepsilon}, \quad (3)$$

where N_0, i, τ_e, and υ represent the sum of q points, the band index, the electron relaxation time, and the electron group velocity, respectively. By semi-classical Boltzmann theory with the constant relaxation approximation, we know that the electrical conductivity can be obtained from σ/τ_e, and τ_e is a constant.[51] It should be noted that the doping level of the system depends on μ within the rigid band model. The positive and negative μ imply n-type and p-type dopings, respectively.

After calculation, we find that the electrical transport properties of Au_2S are isotropic, which results from its perfect lattice symmetry. The Seebeck coefficients of Au_2S only along one direction as a function of μ are illustrated in Fig. 4(a). Obviously, the Seebeck coefficients decrease with the increase

of temperature, which is a typical phenomenon of TE materials. At room temperature, the maximum Seebeck coefficient of Au_2S for p- and n-type dopings are 2.94 mV/K and 2.68 mV/K, respectively, which are particularly higher than those of some well-researched TE materials, such as bulk Cu_2S (0.3 mV/K),[28] $MoSe_2$ (0.9 mV/K),[52] and WSe_2 (0.8 mV/K).[53] The S and DOS satisfy the Mott relation[54]

$$S = \frac{\pi^2 k_B^2 T}{3e}\left\{\frac{1}{n}\frac{\mathrm{d}n(\varepsilon)}{\mathrm{d}\varepsilon} + \frac{1}{\mu_m}\frac{\mathrm{d}\mu_m(\varepsilon)}{\mathrm{d}\varepsilon}\right\}_{\varepsilon=\mu}, \quad (4)$$

where k_B is the Boltzmann constant, n is the carrier density, μ_m is the carrier mobility. It implies that the stair-like PDOS contains several sharp peaks [seen in Fig. 1(b)], which can enhance the carrier concentration $n(\varepsilon)$ and result in high Seebeck coefficient of Au_2S.

The electrical conductivity σ/τ_e along the one direction as a function of μ is depicted in Fig. 4(b). We find that the σ/τ_e of n-type doping is better than that of p-type. This is mainly because for the VBM and CBM, the curvature is different, and the group velocity of the carriers is different. As the curvature of the dispersion curve around VBM is smaller than that of CBM, the transport distribution function of n-type doping in formula (3) is larger than that of p-type, resulting in the σ/τ_e of n-type doping larger than that of p-type. As shown in Fig. 4(c), the κ_e of Au_2S is defined by[55]

$$\kappa_e = L\sigma T, \quad (5)$$

where L is the Lorenz number ($L = \pi^2 k_B^2/3e^2$). Similar to σ/τ_e, κ_e/τ_e has a weak anisotropic as well. Besides, we find that the values of κ_e/τ_e increase with the temperature and the doping, and the n-type doping is better than the p-type one. The power factor relative to the scattering time ($S^2\sigma/\tau_e$) is shown in Fig. 4(d). At room temperature (300 K), the $S^2\sigma/\tau_e$ for p-type doping is higher than that of n-type. But at a higher temperature (500 K and 700 K), it has the opposite result where the $S^2\sigma/\tau_e$ of n-type is higher than that of p-type, which can be attributed to its electrical transport properties.

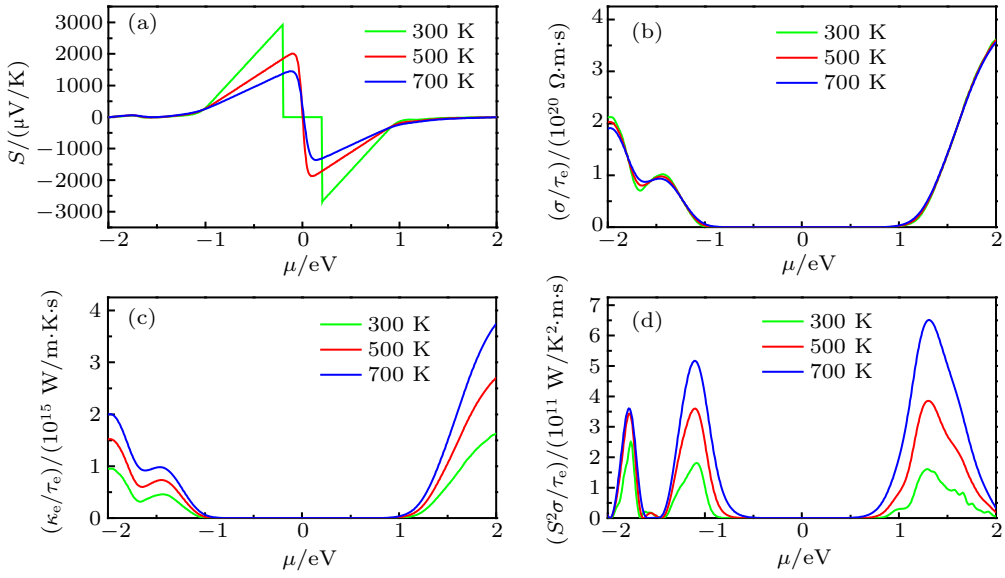

Fig. 4. (a) Seebeck coefficients, (b) electrical conductivity, (c) electronic thermal conductivity, and (d) power factor with respect to the scattering time as functions of the chemical potential μ.

3.3. Thermal transport properties

The phonon dispersion curves and the partial atomic phonon density of states (PhDOSs) for bulk Au_2S are shown in Fig. 5. It is noted that all vibrational modes are found to be positive, indicating the dynamically stable nature at ambient pressure for our system. The Au atoms dominate the low frequency region (below $\sim$ 5 THz), while the high area (from $\sim$ 10.5 THz to 11.8 THz) is mainly contributed by the S atoms. Besides, the low-frequency optical mode crosses the acoustic branch and softens, leading to strong acoustic–optical interactions. This feature is similar to that of some well-known TE materials, such as PbSe,[56] $MoSe_2$, and WSe_2.[57] Form the PhDOS, several peaks can be observed in the optical branch region, which can give rise to the small phonon group velocity. Besides, the relative flat phonon dispersion curves also are beneficial to small phonon velocities, leading to the low lattice thermal conductivity.

The lattice thermal conductivity κ_l is defined as

$$\kappa_{l,i} = \frac{1}{V}\sum_i c_i \upsilon_i^2 \tau_i, \quad (6)$$

where V, c_i, υ_i, and τ_i are the crystal volume of the primitive cell, the model heat capacity, the phonon group velocity, and the phonon relaxation time, respectively. The c_i and υ_i are obtained from the phonon dispersion based on the harmonic 2nd IFCs, and τ_i is obtained from the anharmonic 3rd IFCs. The κ_l of Au_2S, at temperatures from

200 K to 800 K, are shown in Fig. 5(b). At room temperature, the κ_l of Au_2S is about 1.99 $W{\cdot}m^{-1}{\cdot}K^{-1}$, which is smaller than that of bulk $MoSe_2$ (2.32 $W{\cdot}m^{-1}{\cdot}K^{-1}$)[49] and MoS_2 (34.50 $W{\cdot}m^{-1}{\cdot}K^{-1}$).[58] Furthermore, the intrinsic κ_l decreases upon heating. At 700 K, the lattice thermal conductivity is as low as 0.88 $W{\cdot}m^{-1}{\cdot}K^{-1}$. Such low κ_l of Au_2S may originate from its mixture of optical and acoustic branches and relatively flat phonon dispersion curves.

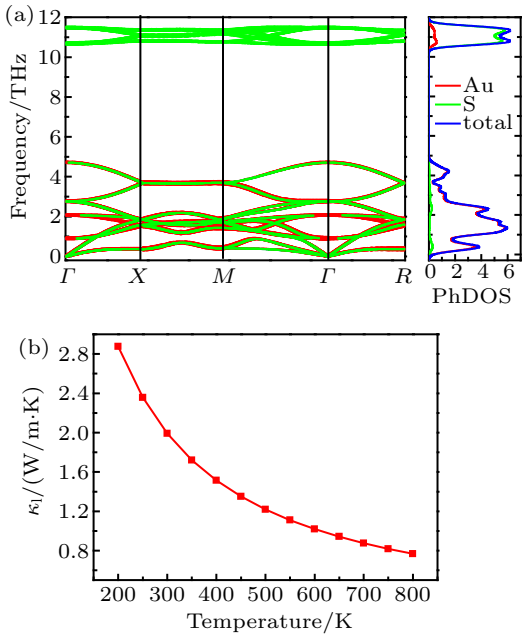

Fig. 5. (a) Phonon dispersion and corresponding total and partial phonon density of states of Au_2S. (b) Calculated lattice thermal conductivity with respect to temperature for Au_2S.

To further understand its low thermal conductivity, we extract the phonon group velocities (ν), Grüneisen parameters (γ), phonon relaxation time (τ), and three-phonon scattering phase space (P_3) with respect to frequency, as shown in Fig. 6. The phonon velocity is calculated by[59,60]

$$\upsilon_\lambda(q) = \frac{\mathrm{d}\omega_\lambda(q)}{\mathrm{d}q}, \tag{7}$$

where $\omega_\lambda(q)$ is the phonon frequency of the phonon mode λ. The Grüneisen parameter is defined as

$$\gamma_\lambda(q) = -\frac{V}{\omega_\lambda(q)}\frac{\partial\omega_\lambda(q)}{\partial V}. \tag{8}$$

It can be seen from Fig. 6(a) that all acoustic phonon modes (ZA, TA, and LA) have higher group velocities than the optical modes. The group velocities of all modes are very low, and the maximum group velocity is less than 2.75 $km{\cdot}s^{-1}$. On the other hand, anharmonicity determines the strength of the three-phonon scattering process. The higher anharmonicity is always related to stronger phonon–phonon interaction, lower group velocity, and lower lattice thermal conductivity. Usually, the γ is used to characterize the anharmonic scattering intensity of phonons. As seen in Fig. 6(b), the acoustic phonon has extremely high γ (about 34 for ZA), which means this system has strong anharmonicity scattering between acoustic phonons. The phonon relaxation time can be acquired by the summation of various scattering processes (umklapp scattering, boundary scattering, and defects scattering). From Fig. 6(c), the TA mode has the longest phonon relaxation time, followed the ZA and optical modes, and then the LA mode. It is worth mentioning that the phonon relaxation time of the LA branch is significantly lower than those of the other three branches, indicating that it has the smallest contribution to the total thermal conductivity.

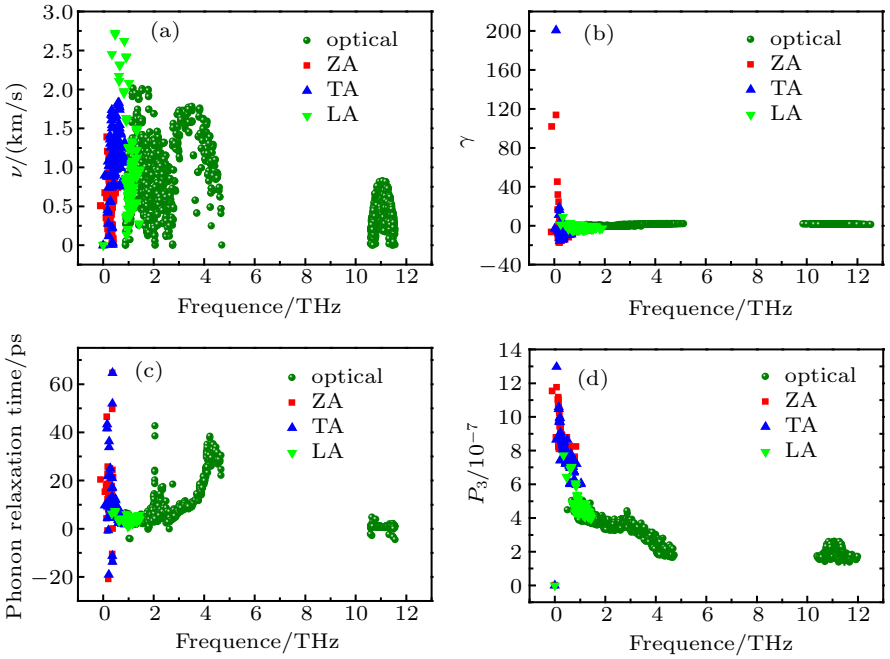

Fig. 6. (a) Phonon group velocities, (b) Grüneisen parameters, (c) phonon relaxation time, and (d) P_3 phase space with respect to frequency for Au_2S.

In addition, the three-phonon scattering phase spaces are used to evaluate the phonon relaxation time of the system. The P_3 can be calculated according to[61]

$$P_3 = \frac{2}{3\Omega}\left(P_3^{(+)} + \frac{1}{2}P_3^{(-)}\right), \tag{9}$$

where Ω is a normalization factor. The large values of P_3 can give rise to the large three-phonon scattering process. Figure 6(d) shows the P_3 of the phonon modes relative to the phonon frequency. It can be seen that the P_3 of the ZA and TA branches are larger than those of the LA branch, which is consistent with their phonon relaxation time. But it cannot be ignored that the P_3 of all acoustic modes are very large, which makes them have strong phonon–phonon scattering and prevents the phonon transport. Through the above analysis, we can well understand the cause of ultra-low thermal conductivity in bulk Au_2S.

3.4. Thermoelectric figure of merit

The ZT of Au_2S can be calculated by combining the phonon and the electron transport coefficients. We present the ZT in Figs. 7(a) and 7(b) as a function of the chemical potential and doping concentration, respectively. Based on the deformation potential (DP) theory,[62] the calculated relaxation time is 2.1×10^{-14} s. Form the formula of ZT, we know that the κ_e has a great influence on ZT. According to our calculated κ_e, we show that the ZT value of the p-type doping is larger than that of the n-type doping. Because of the low lattice thermal conductivity (~ 0.88 W·m^{-1}·K^{-1}) at 700 K, the ZT can approach 1.76. This value is larger than those of many widely studied sulfide materials, such as 0.8 (Cu_xS at 750 K),[63] 0.33, 0.8 (ZrSb at 700 K),[64] and 1.4 (PtTe at 750 K).[65] Such high ZT values indicate that Au_2S is a promising TE material. In addition, the corresponding n-type and p-type doping concentrations in Au_2S to obtain the maximum ZT values at 700 K are approximately 5×10^{20} cm^{-3} and 2×10^{20} cm^{-3}, respectively. Doping at such low concentrations has a slight effect on their phonon and electron structure properties. Overall speaking, Au_2S is a very promising material for TE applications.

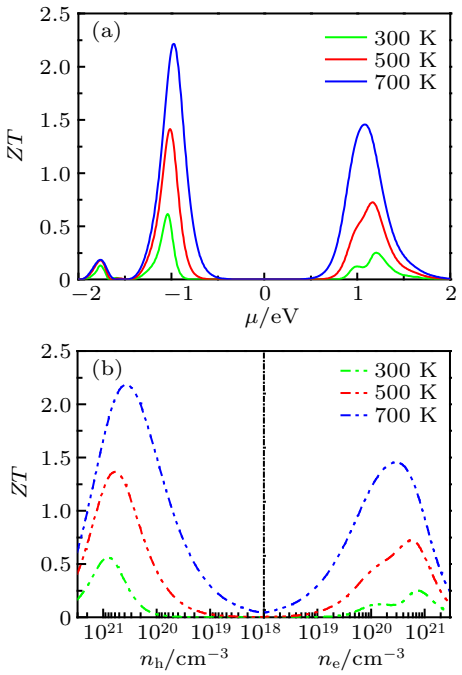

Fig. 7. The thermoelectric figure of merit as a function of (a) chemical potential and (b) carrier concentration for Au_2S at 300 K, 500 K and 700 K.

4. Conclusion

In summary, we studied the TE properties of bulk Au_2S using DFT and Boltzmann transport equation. Results indicate that the thermal transport property and the electrical transport of Au_2S exhibit isotopic behavior. Its small v, large γ, short τ, and large P_3 significantly inhibit phonon transport and lead to low κ_l of 1.99 W·m^{-1}·K^{-1} at room temperature. Highly degenerate VB, peaky DOS, and large Seebeck coefficients (1200 μV·K^{-1}) are observed. The ZT under p-type doping can approach 1.76 at 700 K. Taken together, these results demonstrate the tremendous advantages of bulk Au_2S for efficient thermal energy conversion in the 300 K to 700 K temperature range.

Acknowledgement

The calculations were performed at Supercomputer Center in China Spallation Neutron Source.

References

[1] DiSalvo and Francis J 1999 *Science* **285** 703
[2] He J and Tritt T M 2017 *Science* **357** eaak9997
[3] Sales B C 2002 *Science* **295** 1248
[4] Bell L E 2008 *Science* **321** 1457
[5] Li X, Liu P F, Zhao E, *et al.* 2020 *Nat. Commun.* **11** 942
[6] Zhu X L, Liu P F, Zhang J, Zhang P, Zhou W X, Xie G and Wang B T 2019 *Nanoscale* **11** 19923
[7] Zhang C, de la Mata M, Li Z, Belarre F J, Arbiol J, Khor K A, Poletti D, Zhu B, Yan Q and Xiong Q 2016 *Nano Energy* **30** 630
[8] Zhu X L, Hou C H, Zhang P, Liu P F, Xie G and Wang B T 2020 *J. Phys. Chem. C* **124** 1812
[9] Pei Z, Wang H and Snyder G J 2012 *Adv. Mater.* **24** 6124
[10] Tang L P, Tang L M, Geng H, Yi Y P, Wei Z, Chen K Q and Deng H X 2018 *Appl. Phys. Lett.* **112** 012101
[11] Dun C, Hewitt C A, Li Q, Guo Y, Jiang Q, Xu J, Marcus G, Schall D C and Carroll D L 2017 *Adv. Mater.* **29** 1702968
[12] Zhang Z, Ouyang Y, Cheng Y, Chen J, Li N and Zhang G 2018 *Chin. Phys. B* **27** 035101
[13] Vineis C J, Shakouri A, Majumdar A and Kanatzidis M G 2010 *Adv. Mater.* **22** 3970
[14] Heremans J P, Wiendlocha B and Chamoire A M 2012 *Energy Environ. Sci.* **5** 5510
[15] Zebarjadi M, Joshi G, Zhu G, Yu B, Minnich A, Lan Y, Wang X, Dresselhaus M, Ren Z and Chen G 2011 *Nano Lett.* **11** 2225
[16] Yu B, Zebarjadi M, Wang H, Lukas K, Wang H, Wang D, Opeil C, Dresselhaus M and Chen G and Ren Z 2012 *Nano Lett.* **12** 2077
[17] Soni A, Shen Y, Yin M, Zhao Y, Yu L, Hu X, Dong Z, Khor K A, Dresselhaus M S and Xiong Q 2012 *Nano Lett.* **12** 4305
[18] Mehta R J, Zhang Y, Karthik C, Singh B, Siegel R W, Borca-Tasciuc T and Ramanath G 2012 *Nat. Mater.* **11** 233
[19] Zhu X L, Liu P F, Xie G F and Wang B T 2019 *Phys. Chem. Chem. Phys.* **21** 10931

[20] Tarachand, Hussain S, Lalla N P, Kuo Y K, Lakhani A, Sathe V G, Deshpande U and Okram G S 2018 *Phys. Chem. Chem. Phys.* **20** 5926
[21] Lee E, Ko J, Kim J Y, Seo W S, Choi S M, Lee K H, Shim W and Lee W 2016 *J. Mater. Chem. C* **4** 1313
[22] Androulakis J, Lin C H, Kong H J, Uher C, Wu C I, Hogan T, Cook B A, Caillat T, Paraskevopoulos K M and Kanatzidis M G 2007 *J. Am. Chem. Soc.* **129** 9780
[23] Peng Z, He D, Mu X, Zhou H, Li C, Ma S, Ji P, Hou W, Wei P, Zhu W, Nie X and Zhao W 2018 *J. Electron. Mater.* **47** 3350
[24] Liufu S C, Chen L D, Yao Q and Wang C F 2007 *Appl. Phys. Lett.* **90** 112106
[25] Mulla R and Rabinal M K 2017 *Appl. Surf. Sci.* **397** 70
[26] Ge Z H, Zhang B P, Chen Y X, Yu Z X, Liu Y and Li J F 2011 *Chem. Commun.* **47** 12697
[27] Li X, Hu C, Kang X, Len Q, Xi Y, Zhang K and Liu H 2013 *J. Mater. Chem. A.* **1** 13721
[28] Zhao L, Wang X, Fei F Y, Wang J, Cheng Z, Dou S, Wang J and Snyder G J 2015 *J. Mater. Chem. A.* **3** 9432
[29] Tarachand, Mukherjee B, Saxena M, Kuo Y K, Okram G S, Dam S, Hussain S, Lakhani A, Deshpande U and Shripathi T 2019 *ACS Appl. Energy Mater.* **2** 6383
[30] Zheng Y, Wang S, Liu W, Yin Z, Li H, Tang X and Uher C 2014 *J. Phys. D: Appl. Phys.* **47** 115303
[31] Tan Q, Wu C F, Sun W and Li J F 2016 *Rsc Adv.* **6** 43985
[32] Senftle, Edward F and Wright D B 1986 *Z. Naturforsch. B* **41** 1081
[33] Morris T, Copeland H and Szulczewski G 2002 *Langmuir* **18** 535
[34] Ishikawa K, Isonaga T, Wakita S and Suzuki Y 1995 *Solid State Ionics* **79** 60
[35] Dalmases M, Torruella P, Blanco-Portals J, Vidal A, Lopez-HaroJoséM, Calvino J J, S Estradé PeiróF and Figuerola A 2018 *Chem. Mater* **30** 6893
[36] Kresse G and Furthmüller 1996 *J. Phys. Rev. B* **54** 11169
[37] Blöchl P E 1994 *Phys. Rev. B* **50** 17953
[38] Kresse G and Joubert D 1999 *Phys. Rev. B* **59** 1758
[39] Madsen G K H and Singh D J 2006 *Comput. Phys. Commun.* **175** 67
[40] Chaput L, Pecheur P and Scherrer H 2007 *Phys. Rev. B* **75** 045116
[41] Li W, Carrete J, Katcho N A and Mingo N 2014 *Comput. Phys. Commun.* **185** 1747
[42] Togo A, Oba F and Tanaka I 2008 *Phys. Rev. B* **78** 134106
[43] Suárez J A, Plata J J, Márquez A M and Sanz J F 2016 *Theo. Chem. Acc* **135** 70
[44] Averitt R D, Sarkar D and Halas N J 1997 *Phys. Rev. Lett.* **78** 4217
[45] Zhao L D, Dravid V P and Kanatzidis M G 2014 *Energy Environ. Sci.* **7** 251
[46] Ding G, Wang C, Gao G, Yao K, Dun C, Feng C, Li D and Zhang G 2018 *Nanoscale* **10** 7077
[47] Fu C, Wu H, Liu Y, He J, Zhao X and Zhu T 2016 *Adv. Sci.* **3** 1600035
[48] Alam Hilaal and Ramakrishna S 2013 *Nano Energy* **2** 190
[49] Dehkordi A M, Zebarjadi M, He J and Tritt T M 2015 *Mat. Sci. Eng: R* **97** 1
[50] Gu J, Huang L and Liu S 2019 *RSC Adv.* **9** 36301
[51] Yuan H, Shimotani H, Ye J, Yoon S, Aliah H, Tsukazaki A, Kawasaki M and Iwasa Y 2010 *J. Am. Chem. Soc.* **132** 18402
[52] Brixner L H 1962 *J. Inorg. Nucl. Chem.* **24** 257
[53] Revolinsky E and Beerntsen D J 1964 *Appl. Phys.* **35** 2086
[54] Cutler M and Mott N F 1969 *Phys. Rev.* **181** 1336
[55] Jonson M and Mahan G D 1980 *Phys. Rev. B* **21** 4223
[56] Liu P F, Bo T, Xu J, Yin W, Zhang J, Wang F, Eriksson O and Wang B T 2018 *Phys. Rev. B* **98** 235426
[57] Kumar S and Schwingenschlogl U 2015 *Chem. Mater.* **27** 1278
[58] Yan R, Simpson J R, Bertolazzi S, Brivio J, Watson M, Wu X, Kis A, Luo T, Hight Walker A R and Xing H G 2014 *ACS Nano* **8** 986
[59] Ouyang T and Hu M 2015 *J. Appl. Phys.* **117** 245101
[60] Ouyang T, Xiao H, Tang C, Hu M and Zhong J 2016 *Phys. Chem. Chem. Phys.* **18** 16709
[61] Lee S, Esfarjani K, Luo T, Zhou J, Tian Z and Chen G 2014 *Nat. Commun.* **5** 3525
[62] Xi J, Long M, Tang L, Wang D and Shuai Z 2012 *Nanoscale* **4** 4348
[63] Qiu P, Zhu Y, Qin Y, Shi X and Chen L 2016 *APL Mater.* **4** 104805
[64] Guo Q and Luo S 2015 *Funct. Mater. Lett.* **08** 1550028
[65] Pei Y, LaLonde A, Iwanagaa S and Snyder G J 2011 *Energy Environ. Sci.* **4** 2085